Causal disconnectomics of motion perception: insights from TMS-induced BOLD responses

Short title: BOLD correlates of TMS perturbation in the visual system

Estelle RAFFIN[1,2,3], Roberto F. SALAMANCA-GIRON[1,2], Krystel R. HUXLIN[4], Olivier REYNAUD[5], Loan MATTERA[5], Roberto MARTUZZI[5], Friedhelm C. HUMMEL[1,2,6]

[1] Defitech Chair of Clinical Neuroengineering, Neuro-X Institute (INX), Ecole Polytechnique Fédérale de Lausanne (EPFL), Geneva, Switzerland.

[2] Defitech Chair for Clinical Neuroengineering, INX, EPFL Valais, Clinique Romande de Réadaptation, Sion, Switzerland.

[3] LPNC, CNRS UMR 5105, Université Grenoble Alpes, Saint-Martin-d'Heres, France.

[4] The Flaum Eye Institute and Center for Visual Science, University of Rochester, Rochester, NY, USA.

[5] Human Neuroscience Platform, Fondation Campus Biotech Genève (FCBG), Campus Biotech, Geneva, Switzerland.

[6] Department of Clinical Neurosciences, Geneva University Hospital (HUG), Geneva, Switzerland.

Corresponding Author: Estelle Raffin, LPNC, CNRS UMR 5105,Université Grenoble Alpes, Saint-Martin-d'Hères, France. Email: estelle.raffin@univ-grenoble-alpes.fr. https://orcid.org/0000-0003-3262-5251

Highlights:

- TMS-induced perturbation of the early visual areas (EVA) or the mediotemporal area (MT) area selectively impairs motion direction discrimination.
- The TMS perturbation is associated with a context-dependent local up-scaling of BOLD activity in both areas.
- The two visual areas display distinct topological networks' adaptation in response to TMS, reflecting different levels of network resilience to a focal lesion.
- TMS-fMRI coupling can be used to assess 'causal disconnectomics' and to precisely map how a local perturbation propagates to large-scale behavioural deficits.

Abstract:

Understanding how focal perturbations lead to large-scale network (re)organization is essential for accurately predicting the behavioral consequences of brain lesions. In this study, we applied a 'virtual lesion' approach by means of short bursts of 10 Hz transcranial magnetic stimulation (TMS) over either early visual areas (EVA) or the medio-temporal area (MT) in healthy participants, while acquiring concurrent functional MRI. TMS delivered during the early stages of motion processing selectively impaired direction discrimination at both sites, while global motion perception remained unaffected. These behavioral effects were accompanied by a common local increase in BOLD activity, but distinct patterns of network reorganization. Perturbation of EVA led to more robust and efficient functional adaptation, suggesting greater resilience to focal disruption. In contrast, behavioral impairments following MT stimulation were associated with a less organized, more random network structure. Together, these findings underscore the potential of TMS-fMRI coupling as a powerful approach for mapping *causal disconnectomics*—the dynamic relationships between localized neural disruption and widespread functional and behavioral outcomes providing a better understanding of lesion-induced brain changes in neurological disorders such as stroke.

1. Introduction:

Brain networks dynamically adjust their spatiotemporal organization to changing contexts and ongoing demands (Telesford *et al.*, 2011; Papo *et al.*, 2014). Such adaptive networks can be characterized by their topological transformation, their state-dependency and/or their state transition. The adaptability of brain networks is crucial for maintaining an optimal balance between information segregation and integration, ensuring functional stability, efficient local processing, and communication through long-range connections. Understanding how flexible and distributed brain networks give rise to complex behavior is a central challenge in systems neuroscience. This adaptability may enhance the resilience of functional networks in response to progressive neurodegeneration or focal lesions (Bassett & Bullmore, 2009; Bullmore & Sporns, 2012; Fornito *et al.*, 2015). Today, a comprehensive understanding of the causal relationship between a focal lesion and brain network organization is still missing, leading to the inability to accurately predict resulting symptoms and recovery processes and develop targeted treatment strategies.

Directly testing the systematic association between a focal lesion and brain reorganization in humans is challenging, because of the difficulties in selectively altering activity *in vivo* and decipher the causal impact on brain networks. While advances in neuroimaging have provided detailed descriptions of functional and structural brain connectivity (Lim *et al.*, 2019; Ma *et al.*, 2022; Litwińczuk *et al.*, 2022; Blanco *et al.*, 2024), these correlational approaches offer limited insights into the causal mechanisms that underlie network dynamics and behavior. An emerging approach is to combine non-invasive brain stimulation (e.g., transcranial magnetic stimulation, TMS) with neuroimaging techniques (in particular functional magnetic resonance imaging (fMRI)) (Bergmann et al., 2021; Ozdemir et al., 2020; Vink et al., 2018, Raffin et al., in press). The

combination of TMS with fMRI provides a unique opportunity to temporarily perturb a brain region and assess the changes in local brain activity and the resulting large-scale network responses in vivo that may underlie changes in task performance (Beckers & Hömberg, 1992; Ruff *et al.*, 2006; Bestmann S., 2008; Ricci *et al.*, 2012; Leitão *et al.*, 2015; Cocchi *et al.*, 2016). Several attempts have been made to combine fMRI with TMS to capture the impact that TMS can have on patterns of functional connectivity in specialized, large-scale, brain systems (Ruff *et al.*, 2008; Jung *et al.*, 2020). This holds great promise for establishing *individual causal connectomics* (Glick *et al.*, 2024)— the ability to map the local effects of targeted perturbations of brain nodes and how they propagate across interconnected networks in individual participants.

Despite its conceptual appeal, key physiological mechanisms underlying TMS-fMRI responses remain incompletely understood. First, the local neural response to TMS reflects a complex interplay between intrinsic cortical excitability, synaptic connectivity, ongoing oscillatory activity, and network state. Second, the associated local TMS-evoked BOLD response and its physiological underpinnings remain to be fully elucidated (Rafiei & Rahnev, 2022). However, earlier studies have shown that these local perturbations can propagate through polysynaptic pathways, producing remote BOLD responses that seem to reflect both direct anatomical projections and state-dependent functional interactions (Ruff *et al.*, 2006; Bestmann S., 2008; Siebner *et al.*, 2022). The distinct propagation patterns across brain regions, combined with individual variability, offer a valuable window into mapping subject-specific causal connectivity—*causal connectomics*.

Describing personalized causal connectomics is particularly relevant when considering the application of TMS-fMRI to complex behavioral domains such as perceptual decision-making and motion direction discrimination. Motion direction discrimination is

supported by a distributed network that integrates early visual areas (V1/V2) or EVA (Moore *et al.*, 2001; Koivisto *et al.*, 2010), motion-sensitive temporal regions (MT) (Newsome & Paré, 1988; Liu & Pack, 2017), the intraparietal sulcus involved in sensory evidence accumulation (Chen *et al.*, 2017; Zhang *et al.*, 2022; Wongtrakun *et al.*, 2025), and prefrontal circuits supporting decision-making and response selection (Kennerley & Walton, 2011; Lin *et al.*, 2020). Impairments in this system can arise from dysfunctions at multiple network levels, leading to behavioral deficits that may be difficult to attribute to any single region. Disentangling whether such deficits arise from primary sensory dysfunction, impaired integration, or altered top-down control requires tools that can interrogate how information flows across the network. By applying TMS-fMRI perturbations to key nodes within the motion discrimination network, here to the EVA and MT, it becomes possible to experimentally probe how focal disruptions alter distributed network dynamics and behavior. This approach may ultimately allow us to characterize individual-specific network vulnerabilities that give rise to multidomain symptoms, not only in healthy brain function but also in clinical populations where sensory, cognitive, and motor symptoms often co-occur (Siegel *et al.*, 2016; Fleury *et al.*, 2022; Jimenez-Marin *et al.*, 2022). However, achieving such mechanistic understanding requires further efforts to relate region-specific TMS-evoked local and network-level responses to behavioral outcomes.

In this study, we aim to address these challenges by combining TMS-fMRI perturbation mapping targeting EVA and MT with behavioral assessments of motion direction discrimination, providing novel insights into the causal architecture of perceptual decision-making networks. These two regions were chosen because they allowed us to compare the whole brain consequences of a TMS perturbation affecting a primary integrative brain region, acting as a gateway to other 'higher' visual areas, and in contrast, a more functionally specialized brain region (Simoncelli & Heeger, 1998;

Grossberg *et al.*, 1999; Rust *et al.*, 2006; Mineault *et al.*, 2012). Simulation studies suggest that inhibitory rTMS targeting peripheral regions may exert more pronounced acute changes in network organization than stimulation of hub or integrative regions (Gollo *et al.*, 2017). Accordingly, we hypothesized that, as a primary integrative hub, EVA would display greater local and network-level homeostasis following TMS, thereby attenuating the propagation of perturbation effects and limiting both behavioral impairments and widespread network reconfiguration compared to MT (Das *et al.*, 2012; Gollo *et al.*, 2017; Tu *et al.*, 2021). Therefore, we anticipate that differences in TMS-induced behavioral impairments across behavioral state and across processing stages will be explained by distinct patterns of TMS signal propagation—shaped by the hierarchical network level of the targeted area—rather than by variations in local BOLD responses to TMS.

2. Methods

Participants

In total, thirty healthy subjects (seventeen males: mean age 28.8 years, range 19–39 years) were recruited in the experiment. All participants provided informed written consent prior the experiment and none of them met the MRI or TMS exclusion criteria (Rossi *et al.*, 2021). This study was approved by the local Swiss Ethics Committee (2017-01761) and performed in accordance with the Declaration of Helsinki.

Experimental Design and Task Procedure

155 Sixteen participants (nine males, mean age 26.5 years, range 19-32 years) performed
156 two TMS-fMRI sessions (except one drop-out for the second session). During the first
157 session, TMS was applied to the right EVA ($TMS_{(EVA)}$: mean(±SD) MNI coordinate: 8(5);-
158 76(4);9(6)) using phosphenes perception when possible (in 9/16 participants) or the O2
159 position based on the 10-20 EEG system; during the second session, TMS was applied to
160 the functionally defined right MT ($TMS_{(MT)}$: mean MNI coordinates (SD): 46(4); -83(6);
161 11(5)) (Figure 1A). We chose this study design to maximize our chances to optimally
162 target the individual MT area through a dedicated MT localizer acquired during the first
163 session (see online supplementary materials for a description of the MT functional
164 localizer). For the two online TMS-fMRI sessions, TMS was applied during a *motion*
165 *direction discrimination (MDD) Task* and at *Rest*. These sessions had the same content
166 except the anatomical T1-MPRAGE sequence and the MT functional localizer sequence,
167 which were only performed during the first session. A short offline session prior the MT
168 session was needed to locate the individual MT cluster using a neuro-navigation system
169 (Localite GmbH, Bonn, Germany).

170 An offline control experiment was performed to control for TMS non-specific effects on
171 additional fifteen participants (seven males, mean age 28.9 years, range 22-39 years).
172 We repeated the *MDD task* with TMS using the same setup (neuronavigation and eye-
173 tracking systems) and the same task parameters (see below) but stimulating the right
174 motor cortex ($TMS_{(M1)}$, mean(SD) MNI coordinates: 53(7);-4(2);54(3), corresponding to
175 the individual first dorsal interossei muscle's motor hotspot of the participants), outside
176 the MRI scanner. Figure 1B summarizes the study timeline.

177 For the three sessions, the *MDD task* consisted in rating subjective perceptual
178 experience of visually presented motion stimuli and in performing a forced-choice
179 direction discrimination task on the same moving stimuli (Koivisto *et al.*, 2021). The

180 visual stimuli involved a group of static or moving dots coherently to the right or to the
181 left. During the familiarization phase outside the scanner, the duration of stimulus
182 presentation was individually defined (either 50, 67 or 84 ms, corresponding to 3, 4 or 5
183 frames) to ensure approximatively 70% accuracy in the *noTMS* trials. The stimulus
184 duration was then kept constant throughout the experiment (see Figure 1D for an
185 illustration of the task).

186 Just after the stimulus presentation, participants were asked to rate their perception
187 using a response box with their right hand using a 1 to 4 scale (see Figure 1's caption for
188 more details). In the main experimental conditions, TMS bursts were given to EVA when
189 visual signals first reach the target region 60 ms after the onset of the visual stimulus
190 ($TMS_{(EVA)}$) (Lamme, 2001) and 30 ms after stimulus onset ($TMS_{(MT)}$) for MT to account for
191 the direct thalamic-extrastriate pathway (Beckers & Hömberg, 1992; Lamme &
192 Roelfsema, 2000; d'Alfonso *et al.*, 2002; Koivisto *et al.*, 2010). This ensured similar
193 perturbation of the feed-forward thalamic inputs to the two regions. Later TMS onsets
194 were also tested in half of the trials, 100ms for EVA and 130ms for MT selectively
195 interfering with late processing stages. The total duration of the TMS bursts was 200ms
196 to cover the full window of visual processing in the two regions. TMS intensity was set to
197 ≈ 80% [range: 75 to 90%] maximal stimulator output (MSO), corresponding to dI/dt of
198 119–169 A/ µs. The resulting E-field magnitude at hotspot (99.9-th percentile)
199 corresponded to values between 73 and 112 V/m. This intensity was individually
200 adjusted prior the measurement to ensure phosphene sub-threshold stimulation and
201 progressively increased until participants report pain or discomfort. The intensity was
202 then chosen to get reliable BOLD signal while preserving participant's comfort. For the
203 M1 control experiment, the same EVA timings were used and TMS was given sub-
204 threshold to avoid motor evoked potentials elicitation.

205 Conditions randomly alternated between TMS versus noTMS trials, moving versus static
206 trials throughout the task, 50 trials each, giving a total of 300 trials. An inter-trial interval
207 (ITI) of approximatively 1.5 sec was used. The task was displayed in the scanner through
208 a 44cm x 27cm LCD monitor at a 2.5m distance via a mirror mounted on the head coil,
209 on a frame on top of the TMS-fMRI setup (Figure 1B). For the offline M1 control
210 experiment, the task was displayed on a mid-grey background LCD projector (1024 x
211 768, 144 Hz). To exclude bad performance due to TMS-induced blinking and to make
212 sure that participants were constantly looking at the fixation point, gaze and pupils'
213 movements were controlled in real time with an EyeLink 1000 Plus Eye Tracking System
214 (SR Research Ltd., Canada) in the scanner and in the behavioral room, sampling at a
215 frequency of 1000 Hz. Trials were aborted and redone if deviation exceeded 1° from the
216 fixation point. The duration of the *MDD Task-TMS* sequence was on average 16.5
217 minutes (SD = 4.30 minutes) depending on individual reaction times.

218 A *Rest-TMS* sequence was used to study the effect of TMS intensity. An event-related
219 design was used to map the effect of TMS bursts composed of three pulses at alpha
220 (10Hz) frequency. Three conditions were pseudorandomized and counterbalanced
221 across the run: high-intensity TMS (*HighTMS)*, low-intensity TMS *(LowTMS)* and no TMS
222 *(noTMS),* with 25 repetitions of each condition with an inter-trial interval (ITI) of 6
223 seconds (covering 3 repetition times). *HighTMS* intensity corresponded to the intensity
224 used during the MDD Task while *LowTMS* was set to ≈38 % [35 to 43%] MSO.
225 Participants were asked to look at a fixation cross throughout the acquisition. The
226 duration of the *Rest TMS* sequence was 9 minutes. Note that the results of the Rest-TMS
227 sequence are presented in the supplementary materials.

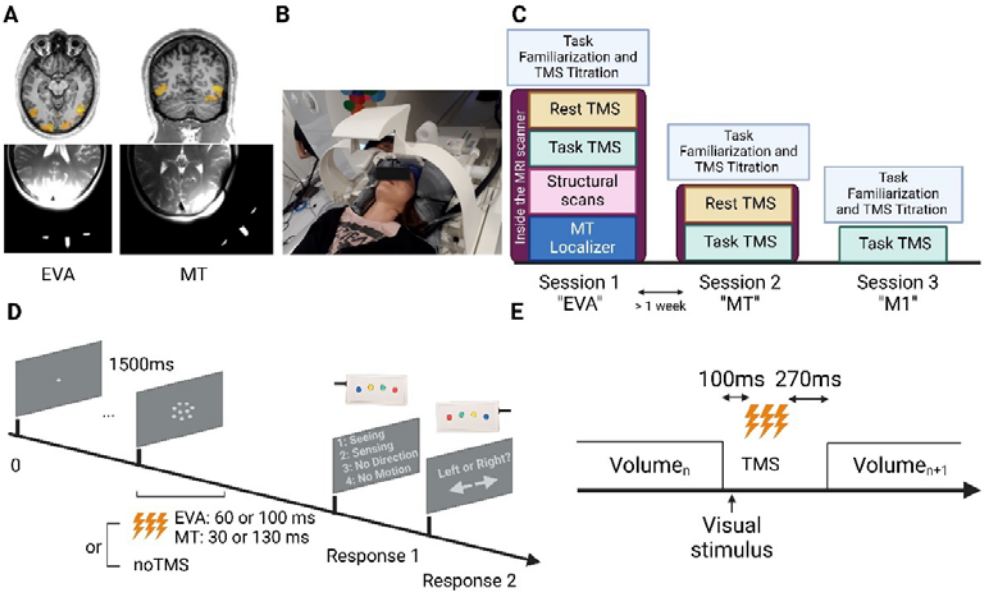

Figure 1.A: TMS targeting*. TMS targets were determined by the functional localizer of EVA and MT for precise TMS positioning (see online materials for further details about the motion processing localizer). The two images on the right part show the T2 image of a representative subject with the oil capsules placed on the TMS-MRI coil casing to monitor the coil position located on the TMS coil for EVA and MT. These markers formed a "T-like shape" indicating the center of the coil as well as the coil orientation as seen on a T2 HASTE image acquired with the two TMS-compatible MRI coil arrays (56 axial slices, slice thickness = 0.8 mm, TR = 1500 ms, TE = 135 ms, FOV = 216 mm, flip angle = 140°).* Coil positions were readjusted if needed. ***B: MRI setup****. The MRI-TMS coil was positioned over the occipital area while the MR-receiving coil was positioned over the frontal lobe. Both were maintained via a vacuum pillow to ensure the absence of movement or vibration and to ensure a comfortable position for the participant.* ***C: Study timeline****: Description of the two experimental sessions;* ***D: One single trial of the motion discrimination task****. The visual stimuli involved a group of white dots in a 5° diameter circular aperture centered in the middle of the screen. The dots were either static or moving coherently to the right or to the left at a density of 2.6 dots per degree. Dots were displayed for 50, 67 or 84 ms (corresponding to 3, 4 or 5 frames). This duration was individually adjusted prior the fMRI measurement to ensure approximatively 70% accuracy in the noTMS trials.* Just after the stimulus presentation, participants were asked to subjectively rate their perception using a response box on their right hand with a 1 to 4 scale, 1 being "I clearly saw the motion" (Seeing), 2 being "I sensed the motion" (Sensing), 3 being "I saw something moving but I'm unable to judge the direction" (No Direction) and 4 being "I didn't see any motion" (No Motion) (Koivisto *et al.*, 2010; Grasso *et al.*, 2018). When the participants pressed the three first options, they were then asked to judge whether the dots moved to the right or to the left with a response box on their left hand. If participants pressed 4, the task moved to the next trial. ***E:*** *Schematic of the BOLD sequence allowing artefact free combination of alpha TMS bursts.*

Behavioral data analysis

258 Considering static stimuli, the mean motion perception accuracy, reflecting how well
259 participants could distinguish between moving and static stimuli, was extracted as the
260 percent of correct answer relative to the total number of trials belonging to the same
261 condition. Using moving stimuli, motion direction discrimination performances were
262 extracted as the percent of correct Left-Right judgments relative to the total number of
263 trials of that condition. For both scores, mixed ANOVA were built with factors Site (EVA,
264 MT and M1) and TMS (Early onset, Late onset and NoTMS). Violation of sphericity was
265 corrected using Greenhouse–Geisser corrections and Tukey's multiple comparisons tests
266 were applied for post hoc analyses when significant main effects or interactions were
267 found.

268

269 ***Magnetic Resonance Imaging & Transcranial Magnetic Stimulation***

270 MRI images were acquired at the Magnetic Resonance Imaging facility of the Human
271 Neuroscience Platform of the Fondation Campus Biotech Genève (FCBG, Biotech
272 Campus, Geneva, Switzerland), using a Siemens Prisma 3 Tesla scanner (Siemens
273 Healthineers, Germany).

274 ***Standard MRI sequences acquisition***

275 Anatomical images were acquired with a 64-channel head and neck coil using a 3D
276 MPRAGE sequence (TR/TE = 2300/2.96 ms, flip angle 9°, 192 sagittal slices, matrix = 256,
277 1x1x1 mm^3 resolution) covering the whole head. For retrospective distortion correction,
278 static field mapping was performed with a double-echo spoiled gradient echo sequence
279 (TR= 652 ms, TE1/TE2=4.92/7.38 ms, resolution 2.2x2.2x2.2 mm^3, whole head coverage),
280 generating two magnitude images and one image representing the phase difference
281 between the two echoes.

282 ***Combined TMS-fMRI sequences acquisition***

283 For combined TMS-fMRI images, two dedicated coil arrays were used (Navarro de Lara
284 *et al.*, 2017). This setup consisted of an ultra-slim 7-channel receive-only coil array,
285 which was placed between the subject's head and the TMS coil (MRI-B91, MagVenture,
286 Farum, Denmark) and connected to a MagPro XP stimulator (MagVenture, Farum,
287 Denmark). A second, receive-only MR coil was positioned over Cz in the EEG 10-20
288 system to allow a full coverage of the participant's brain.

289 The *Rest-TMS* and MDD *Task-TMS* sequences were acquired with a GE-EPI sequence
290 using the same parameters: 40 axial slices, slice thickness = 2.2 mm, in-plane resolution
291 = 2.2 mm, TR = 2000 ms, TE = 30 ms, FOV = 242 mm, flip angle = 67°, GRAPPA = 2,
292 Multiband Factor (MB) = 2. A gap was introduced between consecutive EPI volumes in
293 order to guaranty artefact free MR images after TMS stimulation (Navarro de Lara *et al.*,
294 2015). For both rest and task TMS sequence, a single repetition time (TR=2000 ms) was
295 therefore composed of 40 slices acquired during 1430 ms followed by a gap of 570 ms
296 before the next volume acquisition. The synchronization of TMS pulse was carried out
297 with an in-house script using Matlab (R2019).

298 Static field mapping was also performed with the TMS-MRI coils using the same double-
299 echo spoiled gradient echo sequence (TR = 652 ms, TE = 4.92 and 7.38 ms, slice
300 thickness: 2.2 mm, in-plane resolution = 2.2 mm, flip angle = 60°) that generates two
301 magnitude images and one image representing the phase difference between the two
302 echoes. Additional MRI sequences for coregistration of TMS-fMRI data are described in
303 the supplementary materials.

304

305 ***Preprocessing of fMRI images***

306 Statistical Parametric Mapping software (SPM12, Wellcome Department of Imaging
307 Neuroscience, UK) was used for data pre-processing and analysis of the four datasets
308 (*Rest TMS* and *Task TMS* datasets, on both EVA and MT). Spatial distortions due to field
309 inhomogeneities were removed from all EPI images using the Fieldmap toolbox from
310 SPM12 (Andersson *et al.*, 2001). Subsequently, all time-series were motion-corrected to
311 the first volume using 6 degrees of freedom (3 rotations, 3 translations) and drifts in
312 signal time courses were corrected as well. To improve the normalization procedure,
313 two intermediate steps were added (see online materials for further details about the
314 additional sequences used for coregistration purposes). A first co-registration was
315 performed between the mean realigned and slice timing corrected image and the SSFP
316 sequence acquired with the same MR coil (and thus the same spatial coverage). The
317 resulting, co-registered image was once more co-registered to the SSFP sequence
318 acquired with the MR coil integrated into the scanner (i.e., the body coil, thus preserving
319 the contrast). The latter could then be easily co-registered to the high resolution T1
320 image acquired with the 64-channel head coil that covered the whole brain, and later
321 transformed into standard MNI space using a segmentation-based normalization
322 approach (Ashburner & Friston, 2005). Finally, the normalized images were spatially
323 smoothed using a Gaussian kernel (4 mm, Full-width half-maximal). The realignment
324 parameters estimated during spatial pre-processing for the *Rest TMS* and *Task TMS*
325 dataset were introduced in the design matrix as regressors of no interest in order to
326 prevent confounding activations related to minor head movements during scanning. The
327 experimental event-related designs were convolved with the canonical hemodynamic
328 response function, and the resulting models described in the following section were
329 estimated using a high-pass filter at 128 s to remove low-frequency artefacts.

330

fMRI Univariate Analysis

EVA and MT datasets were similarly analyzed using general linear models (GLM) to calculate individual contrasts. For the *Task TMS* sequence, a design matrix with TMS conditions (TMS_{early}, TMS_{late}, *noTMS*) and visual state (*Moving*, *Static*) was constructed using all trials. To disentangle the effects of a TMS onsets and visual stimuli, we built GLM with random effects at the second-level, by calculating a flexible factorial design, as implemented in SPM12, with the within-subject factors *TMS condition* (TMS_{early}, TMS_{late}) and *Visual stimulus* (Moving and Static).

To explore the local effects of TMS across conditions, mean beta values were extracted from the stimulated regions EVA and hMT+/V5 defined as a 8 mm radius sphere based on the results of the group-level analysis of the motion processing localizer (supplementary online materials) using the MarsBaR toolbox (Brett *et al.*, 2002)(right EVA: 6, -83, 11 and right MT: 58, -66, -3). Repeated measure ANOVAs were built with TMS (TMS_{early}, TMS_{late}, *noTMS*) and visual stimulus (*Moving*, *Static*) as within-subject factors for each site of stimulation (EVA and MT).

For the *RestTMS* sequence, we defined a design matrix comprising three conditions (*HighTMS*, *LowTMS* and *noTMS*). A second-level GLM with random effects was designed using a flexible factorial design, with the within-subject factors *TMS intensity* (TMS_{High}, TMS_{Low} and *noTMS).* Beta values were extracted locally for each condition using the same ROI as previsouly described.

The statistical significance threshold was set to a height threshold of $p < 0.001$ uncorrected, at the voxel level and to that of $p < 0.05$ at the cluster level after false-discovery rate (FDR) correction.

355 ***fMRI Multivariate Analysis:***

356 Independent Component Analysis (ICA) was used on the motion discrimination task
357 data to estimate independent spatiotemporal functional networks from the data and to
358 visualize networks specifically modulated by TMS. ICA uses fluctuations in BOLD signal to
359 split it into maximally independent spatial maps or components, each explaining a
360 unique part of variance from the 4D fMRI data. Then, all components have their specific
361 time course related to a coherent neural signal potentially associated with intrinsic brain
362 networks, artifacts, or both. The group ICA of fMRI Toolbox (GIFT version 3.0b; (Calhoun
363 *et al.*, 2001)) was used. First, it concatenates the individual data followed by the
364 computation of subject-specific components and time course. Maximum Description
365 Length (MDL) and Akaike's criteria were applied to estimate the number of ICs in our
366 data. Using principal component analysis, individual data was reduced. Then, the
367 informax algorithm (Bell & Sejnowski, 1995) was applied for the group ICA and
368 estimated 16 components. In order to improve the IC's stability, the ICASSO was applied
369 and run 20 times (Himberg *et al.*, 2004). Over the 8 extracted network components, we
370 focused on the TMS specific networks defined by the overlap between the activated
371 clusters and the coordinates of the stimulation target. Based on these independent
372 components, we then examined how each condition (Moving or Static) covaries with the
373 TMS networks using the *temporal sorting* option in the GIFT toolbox. Temporal sorting
374 consists in regressing the fMRI specific time course for each individual against the design
375 matrix for the experimental conditions. The resulting betas weights represent the
376 degree to which network was recruited by the conditions. For a network, positive and
377 negative b weights indicate the level of network recruitment in each experimental
378 condition. Paired-sample t-tests were used to identify networks that were significantly
379 modulated by TMS at rest and during motion discrimination using $p < 0.05$.

380 ***Brain Networks generation and Graph Theoretical Analysis***

381 In addition to ICA, we used the graph theoretical network analysis toolbox GRETNA to
382 image connectomics and construct the functional brain networks derived from the full
383 Task $TMS_{(EVA)}$ and $TMS_{(MT)}$ dataset comprising all the conditions of interest (e.g., noTMS,
384 TMS, motion or static stimuli) (Wang *et al.*, 2015). The whole brain was divided into 90
385 cortical and subcortical regions according to Automated Anatomical Labeling (Tzourio-
386 Mazoyer *et al.*, 2002), and the mean time series for each of the 90 regions was
387 extracted. Pearson's correlation coefficients for each pair of regions were calculated for
388 the mean time series of all of the 90 regions, and z-transformed using Fisher's Z
389 transformation. Subsequently, a positive binary undirected connection functional
390 network was constructed according to a range of selected threshold of the relation
391 matrix. As there is no defined standard for threshold selection in the construction of a
392 binary connection brain functional network, sparsity was used as a range of correlation
393 coefficient thresholds for correlation metrics. It was defined as the existing number of
394 edges in a graph divided by the maximum possible number of edges. In accord with
395 previous studies, we set both the sparsity and Pearson correlation threshold of the
396 functional network to range from 0.05 to 0.5 (in 0.05 steps), resulting in a more efficient
397 functional network than a random network with the number of artificial edges
398 minimized (Achard & Bullmore, 2007; Zhao *et al.*, 2017). Graph theoretical analysis was
399 applied to assess the topological and organizational properties focusing on 3 graph
400 theoretical metrics (Rubinov & Sporns, 2010). These metrics were: the clustering
401 coefficient (γ), which measures how much neighbors of a node are connected to each
402 other and is closely related to local efficiency; characteristic path length (λ), which is the
403 average number of edges needed to get from any node in the network to any other
404 node in the network and is inversely related to global efficiency; small worldness (δ),
405 which reflects whether the network balances global integration and local segregation for

efficient information processing (Latora & Marchiori, 2001). To compare graph theoretical network properties between EVA and MT, integration of the topological metric over all selected ranges of sparsity values was calculated using GRETNA. Paired t-tests corrected for FDR ($p < 0.05$) were performed between the topological measures of EVA and MT networks.

3. Results

3.1 Behavioural results

We used chronometric TMS-fMRI coupling in healthy participants to perturb and map the effect of TMS over the right EVA ($TMS_{(EVA)}$) and over the right MT ($TMS_{(MT)}$) during a motion direction discrimination task. An additional offline experiment targeted the right primary motor cortex ($TMS_{(M1)}$) in another subgroup of healthy participants.

Figure 2A shows the mean and individual motion perception accuracy (+/- SEM), reflecting how well participants could distinguish between moving and static stimuli when a TMS burst was applied over EVA (top row), MT (middle row) and over the control region M1 (bottom row). A mixed ANOVA revealed no main effect of TMS ($F_{(1,24)} = 2.9$, $p = 0.084$, $\eta^2 = 0.02$) and no significant TMS by Site interaction ($F_{(4,48)} = 0.9$, $p = 0.452$, $\eta^2 = 0.031$), suggesting that TMS has no consequence on motion perception in these three regions. However, there was a Site effect ($F_{(2,24)} = 6.8$, $p = 0.004$, $\eta^2 = 0.16$), likely driven by the overall better performances in the M1 session. The same model applied to the motion direction discrimination performances (Figure 2B) revealed a significant TMS effect ($F_{(2,305)} = 22.012$, $p < 0.001$, $\eta^2 = 0.2$) and Site effect ($F_{(2,30)} = 20.57$, $p < 0.001$, $\eta^2 = 0.2$). There was also a TMS by Site interaction ($F_{(4,60)} = 9.87$, $p < 0.001$, $\eta^2 = 0.124$). When TMS was applied to EVA, performances were markedly affected by TMS_{early} compared to noTMS ($t_{(15)} = 5.2$, adjusted $p < 0.001$) and compared to TMS_{late} ($t_{(15)} = 4.4$,

adjusted $p = 0.034$). Although slightly lower, the difference between noTMS and TMS_{late} was not significant ($t_{(15)} = 1.45$, $p = 0.35$).

In contrast, when applied to MT, TMS_{early} and TMS_{late} negatively impacted performance compared to noTMS (TMS_{early}: $t_{(15)} = 5.2$, adjusted $p < 0.001$, TMS_{late}: $t_{(15)} = 5.2$, $p < 0.001$). After correction for multiple comparisons, performance under TMS_{early} and TMS_{late} were not different ($t_{(15)} = 2.2$, $p = 0.1$). Performances were similar in the three TMS conditions for M1 (all comparisons $p>0.05$) and baseline performances (noTMS conditions) were not different across sites (all comparisons $p>0.05$).

We also examined the relationship between awareness and accuracy by taking into account motion awareness ratings (see supplementary Figure S1). Without TMS, motion direction discrimination increased (moved away from chance level) as subjective awareness of motion increased. This indicates that without TMS, performance is tied to conscious motion awareness. The rmANOVA with TMS and Rating as within subject factors only revealed a significant Site by TMS condition interaction, confirming the previous analysis ($F_{(4,12)} = 15.1$, $p < 0.011$, $\eta^2 = 0.09$). There was no main effect of Awareness nor interactions with any other factor (all $p>0.05$).

In summary, TMS bursts exerted negative effects on motion direction discrimination at the early and late onsets in MT. TMS bursts were only efficient in disturbing motion directions discrimination in the early onset for EVA. The two onsets did not affect performances when targeting the control region M1.

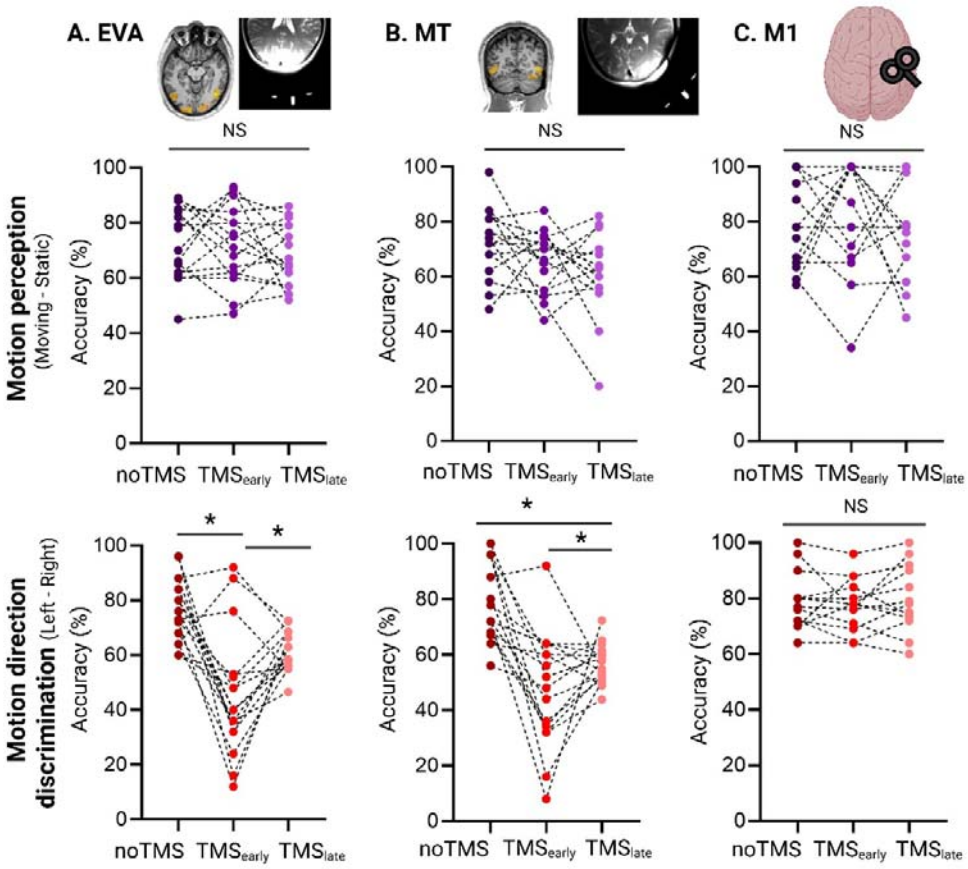

Figure 2: *The upper row illustrates the individual data of motion perception under noTMS, TMS_{early} and TMS_{late} for $TMS_{(EVA)}$ (A), $TMS_{(MT)}$ (B) and $TMS_{(M1)}$ (C); The bottom row illustrates the individual data of motion direction under noTMS, TMS_{early} and TMS_{late} for $TMS_{(EVA)}$ (A), $TMS_{(MT)}$ (B) and $TMS_{(M1)}$ (C);*

3.2 Whole-brain and local responses to TMS perturbation

Next, we analyzed local BOLD activity in response to TMS bursts over EVA and MT applied during behavioral perturbation of motion direction discrimination. First, Figure 3A ($TMS_{(EVA)}$) and Figure 3B ($TMS_{(MT)}$) report the results of the average effects of TMS conditions. $TMS_{(EVA)}$ induced significant clusters in the bilateral occipital cortex, the right superior and middle temporal gyrus, in the bilateral anterior and middle cingulate cortex, the left middle frontal gyrus, the bilateral caudate nucleus and in the right posterior thalamus. When TMS was given over the right MT, the average effect of TMS conditions returned significant clusters in the right occipital cortex, the right inferior and frontal gyrus, the right intra-parietal sulcus and the right cerebellum (cruz VI). These

468 clusters overlapped with the TMS-induced activation at rest (see supplementary results
469 and Table S1).

470 We then examined the main effect of visual stimuli (difference between TMS
471 applied during a moving or static stimuli) returned significant clusters in the right middle
472 temporal gyrus and in the bilateral middle frontal gyrus the right superior frontal gyrus,
473 the posterior cingulate cortex, and the right occipital cortex when EVA was stimulated
474 (Figure 3C) and only in the right middle temporal gyrus, when MT was stimulated (Figure
475 3D). When stimulating the EVA, the main effect of TMS onsets revealed a significant
476 cluster in the right middle frontal gyrus and in the right superior frontal gyrus (Figure
477 3E). There was no significant cluster when stimulating MT (see Supplementary Table S2
478 and S3 for the MNI coordinates of the significant clusters of all effects).

479 The extracted beta values from the stimulated EVA and MT regions were
480 entered into an ANOVA with the factors TMS (noTMS, TMS_{early} and TMS_{late}) and Visual
481 stimuli (moving, static) and stimulation site (EVA, MT). This analysis revealed a
482 significant TMS effect ($F_{(2,22)} = 3.8$, $p = 0.038$), mostly driven by an increase in beta
483 weights for the two TMS conditions compared to no TMS, while there was no difference
484 between the early and late TMS onsets. Finally, there was a significant TMS by Visual
485 stimuli interaction ($F_{(2,22)} = 6.1$, $p = 0.008$) showing that the increase in activity only
486 occurred in the combination early TMS associated with moving stimuli (noTMS, Moving
487 vs early TMS, Moving: $t_{(12)} = -4.2$, $p = 0.003$ and early TMS, Static vs early TMS, Moving:
488 $t_{(12)} = -3.6$, $p = 0.015$, supplementary Table S4 for all posthoc comparisons). There was no
489 stimulation site effect, demonstrating that the local response to TMS were similar in
490 both regions.

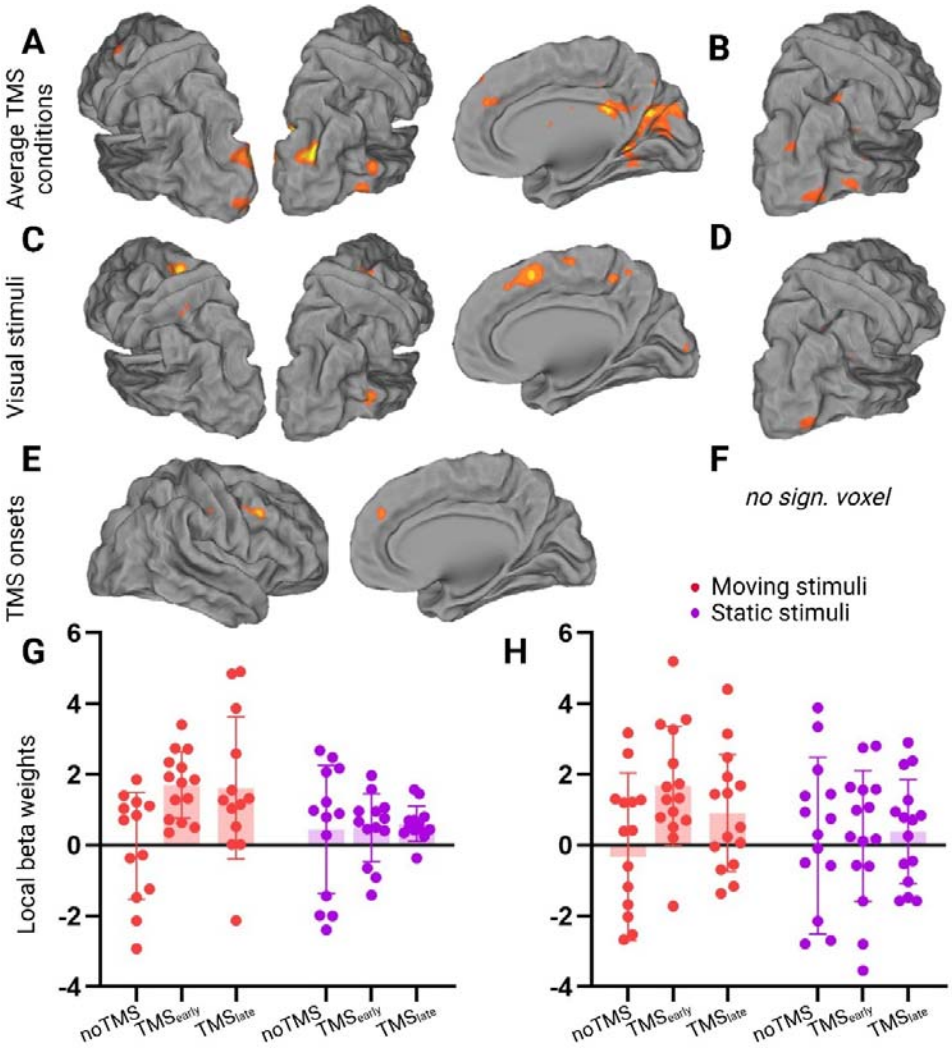

Figure 3A: *Activation maps corresponding to the average TMS conditions for $TMS_{(EVA)}$;* ***B:*** *Activation maps corresponding to the average TMS conditions for $TMS_{(MT)}$;* ***C:*** *Main effect of visual stimuli for $TMS_{(EVA)}$;* ***D:*** *Main effect if visual stimuli for $TMS_{(MT)}$;* ***E:*** *Main effect of TMS onsets for $TMS_{(EVA)}$;* ***F:*** *Main effect of TMS onsets for $TMS_{(MT)}$;* ***G:*** *Local beta weights extracted for the EVA ROI:* ***H:*** *Local beta weights extracted for the MT ROI. P(FWE)) < 0.001 at the cluster level.*

3.3 Network changes in response to TMS perturbation

We further investigated whether and how long-range brain activity was modulated by TMS during motion direction discrimination. We first applied an independent component analysis to extract hidden spatiotemporal components contained within the $TMS_{(EVA)}$ and $TMS_{(MT)}$ task data, returning a measure of functional connectivity. We then

503 applied temporal regression analysis on the components' time courses to compare
504 network activity associated with the different experimental conditions.

505 The ICA applied to the $TMS_{(EVA)}$ data during motion discrimination revealed 8
506 independent networks, among which 7 were considered as functional brain networks.
507 Five networks (IC1, IC3, IC4, IC7 and IC8) were labelled as TMS-related networks because
508 they overlapped with the stimulation site (Figure 4A and Supplementary Table S5 for the
509 MNI coordinates of the IC). IC1, IC7 and IC8 covered the bilateral EVA while IC3 only
510 encompassed the right EVA and IC4, the left EVA. Only IC1 and IC7 were significantly
511 modulated by TMS as revealed by one-way ANOVAs modeling the t scores obtained
512 from the temporal regression analysis on the components' time courses for moving and
513 static stimuli. IC1 was significantly down regulated by both TMS onsets when associated
514 with moving stimuli only (one-way ANOVA: $F_{(2,15)} = 3.6$, $p = 0.04$, post hoc TMS_{early} vs
515 noTMS: $t_{(15)} = 1.9$, $p = 0.07$, TMS_{late} vs noTMS: $t_{(15)} = 2.2$, $p = 0.04$). IC7 showed a different
516 pattern of modulation reflecting a significant over-expression of the bilateral EVA only
517 during TMS_{early}, for moving ($F_{(2,15)} = 3.5$, $p = 0.045$, post hoc TMS_{early} vs noTMS: $t_{(15)} = 2.4$,
518 $p = 0.03$) and static stimuli ($F_{(2,15)} = 4.4$, $p = 0.03$, post hoc TMS_{early} vs noTMS: $t_{(15)} = 2.3$, p
519 = 0.035). All the other ANOVAs were not significant.

520 When TMS was given over MT, 7 components were considered as functional brain
521 networks. Among them, three networks (IC1, IC2 and IC8) were labelled as TMS-related
522 networks (see Supplementary Table S6 for the MNI coordinates of the IC). Interestingly,
523 these networks were not only restricted to the right MT. IC2 and 8 also included the IPS
524 and superior parietal cortex and the medial frontal gyrus. IC 1 activity was significantly
525 enhanced by both TMS onsets when stimuli were moving ($F_{(2,15)} = 3.6$, $p < 0.001$ post hoc
526 TMS_{early} vs noTMS: $t_{(15)} = 2.7$, $p = 0.02$, TMS_{late} vs noTMS: $t_{(15)} = 3.8$, $p = 0.002$) while IC8
527 was significantly depressed during moving stimuli ($F_{(2,15)} = 7.4$, $p = 0.003$, post hoc

528 TMS_{early} vs noTMS: $t_{(15)} = 3.2$, $p = 0.007$, TMS_{late} vs noTMS: $t_{(15)} = 3.1$, $p = 0.008$, Figure 4B).

529 All the other ANOVAs were not significant.

530

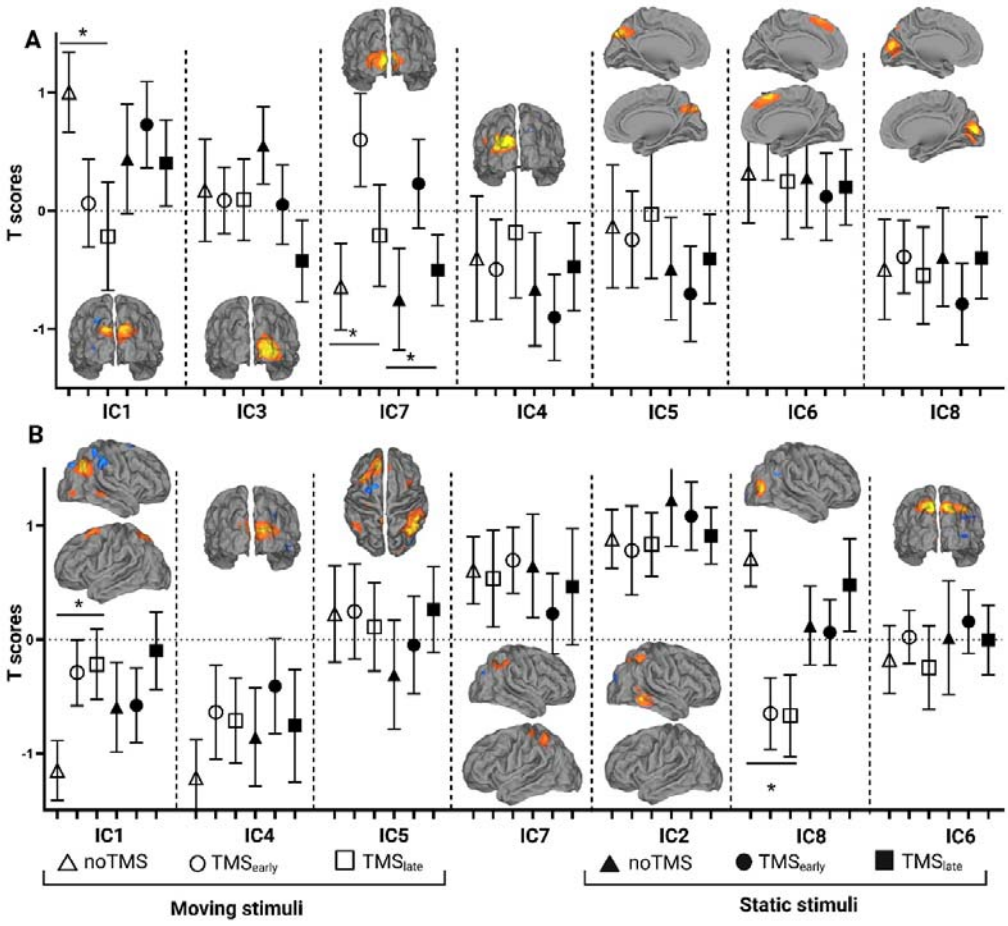

531

532 ***Figure 4A**: $TMS_{(EVA)}$-specific component networks that are modulated by TMS during motion*
533 *discrimination and temporal regression analysis for the noTMS and $TMS_{(EVA)}$ conditions associated*
534 *with moving or static stimuli; **B:** $TMS_{(MT)}$-specific component networks that are modulated by TMS*
535 *during motion discrimination and temporal regression analysis for the noTMS and $TMS_{(EVA)}$*
536 *conditions associated with moving or static stimuli; Note that the components are sorted based*
537 *on the percent of explained variance.*

538

539 Finally, we used a graph theoretical analysis to assess the topological and organizational

540 properties of these networks, while being agnostic to the TMS condition and visual

541 stimulus. We first investigated small-world topological properties especially because

542 networks with high small-world properties are believed to play a role in protecting the

brain from local perturbation or damage. Both EVA and MT networks exhibited small-world properties ($\lambda \approx 1$ and $\sigma > 1$) among the selected sparsity values (see Methods section). Interestingly, there was a significant difference in the small-world network parameters (Sigma) between EVA networks and MT networks with higher Sigma values for EVA networks at the sparsity values 0.3, 0.4, 0.45 and marginally at 0.35 (Figure 5A, left panel and supplementary Table S7 for all paired t-tests), also considering the mean across all sparsity values ($t_{(12)} = 2.4$, $p = 0.034$) (Figure 5B, left panel). There was no difference in normalized clustering coefficient (Gamma) ($t_{(14)} = 0.42$, $p = 0.68$) (Figure 5A & B, middle panels and supplementary Table S8 for all paired t--tests). Finally, characteristic path length (Lambda) was significantly higher at sparsity thresholds of 0.2, 0.25 and marginally at 0.15 for MT networks (Figure 5A, right panel and supplementary Table S9 for all paired t-tests). The difference between EVA and MT+/ networks was also significant when averaging across scarcities ($t_{(14)} = 2.4$, $p = 0.03$, Cohen's d: 0.75) (Figure 5B, right panel).

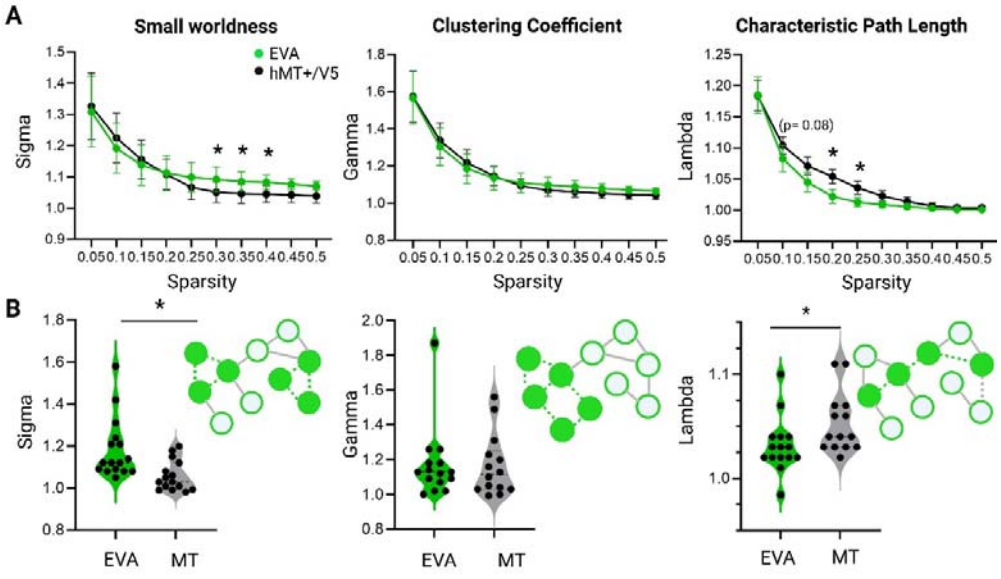

***Figure 5A**: Small-worldness properties (left panel), normalized clustering coefficients (middle panel) and normalized characteristic path length (right panel) for $TMS_{(EVA)}$ and $TMS_{(MT)}$ along the sparsity thresholds of 0.05-0.50; **B:** Associated mean values of small-worldness properties (left panel), normalized clustering coefficients (middle panel) and normalized characteristic path length (right panel) for $TMS_{(EVA)}$ and $TMS_{(MT)}$ * $p < 0.05$.*

3.4 Predicting TMS effects on behaviour with BOLD activity

To explain the effect of TMS on motion direction discrimination, we performed a series of multiple linear regressions using for each of the four conditions ($TMS_{(EVA)}$early, $TMS_{(EVA)}$late, $TMS_{(MT)}$early, $TMS_{(MT)}$late), the associated local beta scores, the t scores derived from the temporal regression of the significant TMS-ICs and the three graph theory metrics as fixed effects. The significant model explained the drop in performance associated with $TMS_{(MT)}$early with Gamma values from the graph theory analysis as confirmed by the ANOVA on the model's parameters ($F_{(1,6)} = 6.6$, $p = 0.04$), suggesting that TMS exerted a negative impact especially in participants showing lower cluster coefficient, implying a more random or decentralized network structure. All other models were not significant (see supplementary Table S10 for all the multiple linear regressions results).

578 # 4. Discussion

579 The goal of this study was to examine whether TMS perturbation elicits inter-
580 individual differences in BOLD responses, potentially reflecting the magnitude of the
581 induced behavioral impairment. We used short bursts of 10Hz TMS to disrupt either a
582 low-level visual area (EVA) or a highly specialized, motion sensitive, visual area (MT)
583 during concurrent fMRI. We first confirmed the causal involvement of both regions in
584 motion direction discrimination, with more pronounced behavioral impairments
585 following stimulation of MT. Our main findings were: (1) a local, context-dependent
586 increase in BOLD activity common to both targeted areas; (2) distinct patterns of
587 network reconfiguration; and (3) a relationship between TMS-induced performance
588 decline after MT stimulation and a shift toward a more random network structure.
589 These results suggest that TMS perturbation triggers area-specific topological
590 adaptations, which may reflect differing levels of network resilience to focal disruption.

591

592 **4.1. TMS-induced behavioural deterioration**

593 In line with the concept of "virtual lesion" described in the literature (Pascual-
594 Leone *et al.*, 1999; Beynel *et al.*, 2019), TMS bursts applied to either EVA and MT,
595 resulted in a selective and transient deterioration of performance of a left/right motion
596 direction discrimination task (except for the late $TMS_{(EVA)}$ condition). This was
597 interpreted to reflect successful causal and selective disruption of brain functioning.
598 Interestingly, participants remained able to dissociate moving from static stimuli. This
599 dissociation is likely supported by the existence of independent substrates mediating
600 unspecific motion processing versus global motion direction integration in EVA and MT
601 (Simoncelli & Heeger, 1998). There is evidence showing that a sub-population of

602 neurons in MT focuses on the processing of local motion signals similar to that in EVA,
603 and some other neuronal populations rather process global motion (Born & Tootell,
604 1992). Our TMS perturbation might have specifically impacted on the neurons in charge
605 of motion directions decoding. The absence of significant impairment induced by the
606 late onsets of $TMS_{(EVA)}$ might be explained by different time delay of feedback loops in
607 the motion discrimination system (Foss & Milton, 2000; Joukes *et al.*, 2014). Considering
608 now the relationship between motion awareness and motion direction discrimination
609 (please see supplementary Figure SX), we found that the direction of the moving trials
610 that were judged as "moving", were not correctly guessed when both areas were
611 stimulated. In contrast, "unaware" trials were unchanged. We can speculate that this
612 residual, unconscious ability of detecting changes in the dots' positions might be at least
613 partially supported by the activation of the fast, direct geniculo-extra-striate pathway
614 (Bridge *et al.*, 2008; Ajina *et al.*, 2015; Abed Rabbo *et al.*, 2015).

615

616 **4.2. Local TMS-induced activity**

617 Our results demonstrate that short bursts of TMS can elicit local BOLD activation
618 beneath the coil in both EVA and MT, even at relatively low intensities—below the
619 phosphene threshold. While the presence of local BOLD activity elicitation in response
620 to TMS is still unresolved in the field (Rafiei & Rahnev, 2022), we specifically found a
621 local over-activation in the presence of moving visual stimuli for both regions. This
622 coupling between local BOLD increase and decreased performance suggests that the
623 additional activity may reflect the accumulation of task-irrelevant neural noise (Ruff *et*
624 *al.*, 2009; Bancroft *et al.*, 2014). Such a mechanism aligns with established models of
625 TMS-induced disruption, where stimulation is thought to activate neuronal populations
626 that are not optimally tuned to the task-relevant feature—in this case, motion direction

(Silvanto & Pascual-Leone, 2008). As a result, the effective signal-to-noise ratio within the motion-sensitive network would be reduced, impairing accurate motion discrimination. It also highlights the state-dependent nature of TMS effects: stimulation during active motion direction processing leads to qualitatively different outcomes than during static stimuli presentation, suggesting that the excitability and engagement of the targeted network at the time of stimulation critically shape the neuronal consequences. These findings reinforce the idea that TMS does not simply "excite" or "inhibit" local tissue, but interacts dynamically with ongoing neural activity (Romero *et al.*, 2019; Siebner *et al.*, 2022). This, together with other recent findings (Perera *et al.*, 2024; Luo *et al.*, 2025), might open the door to more tailored or context-sensitive brain stimulation protocols.

3. TMS induced whole-brain activity

An important question is whether this “local noise injection” propagates in the brain to destabilize larger functional networks. TMS-induced changes in BOLD activity were observed not only locally in the stimulated regions, but also in remote areas through functional coupling. For both EVA and MT stimulation, the spread of activity to distal regions—such as the intraparietal sulcus (IPS), frontal eye fields (FEF), and medial prefrontal cortex—replicates previous findings from TMS-fMRI studies (Ruff *et al.*, 2006; Caparelli *et al.*, 2010; Leitão *et al.*, 2015). Notably, many of these remote regions are task-relevant and are known to be engaged during motion perception and direction discrimination (Offen *et al.*, 2010; Sani *et al.*, 2021), suggesting that the ongoing task context may also shape the propagation of TMS-evoked activity through the actively engaged network.

When TMS was applied during motion processing, additional BOLD activation was observed in regions such as the medio-temporal cortex (including MT) and medial frontal areas. Importantly, this increased activation coincided with a measurable decline in behavioural performance on the motion direction discrimination task, as well as with participants' subjective reports of increased task difficulty. These findings suggest that TMS may disrupt efficient network integration during perceptual processing, potentially by altering the balance of activity within task-relevant networks. The differential effect induced by the early and late TMS onsets was only visible when stimulating EVA and manifested as an increase in activity in the right FEF and in the medial prefrontal cortex with the late onsets. These regions are involved in perceptual decision making and this time could reflect a compensatory mechanism that maintain stable performance (Imani *et al.*, 2021).

4. TMS-induced network activity

To provide both a qualitative and quantitative framework for comparing network activity across different TMS-induced perturbation, we combined group Independent Component Analysis (ICA) with graph-theoretical metrics. ICA identified multiple functional networks, some directly linked to TMS and others more domain-general. Across both targeted regions (EVA and MT), the decomposition revealed components with divergent responses to TMS. In the case of EVA, for example, IC7—spatially overlapping with the site of stimulation—showed increased activation specifically following early TMS onset. In contrast, IC1, located more rostrally, exhibited a pattern of downregulation under the same stimulation condition. The opposing responses may reflect a balance between excitatory and inhibitory processes, possibly mediated by intra-areal or feedback projections (Shao & Burkhalter, 1996; Schwabe *et*

676 *al.*, 2006). Furthermore, the specificity of IC7's response to early TMS onset raises
677 questions about the temporal dynamics of network susceptibility, with different
678 networks or nodes having critical windows of "vulnerability" or influence (Huang & Yu,
679 2017; Kottaram *et al.*, 2018). This dissociation suggests that ICA successfully captured
680 the complex, spatially and temporally differentiated dynamics of TMS-induced
681 responses. It highlights ICA's sensitivity not only to spatial localization but also to the
682 functional state of the network—whether it is task-relevant, engaged, or modulated by
683 TMS in a context-dependent manner. It further emphasizes that TMS effects are not
684 uniform within a target region but depend on the local functional architecture and
685 current cognitive or perceptual state.

686 Regarding network activity induced by $TMS_{(MT)}$, we found that TMS engaged
687 more spatially distributed networks, involving additional associative regions such as the
688 FEF, the posterior parietal cortex (PPC), and medial prefrontal cortex (mPFC). In
689 contrast, all but one of the independent components associated with $TMS_{(EVA)}$ were
690 largely confined to the stimulated visual area, indicating more localized network
691 engagement.

692 To quantitatively assess these differences, we applied graph-theoretical analyses
693 and observed distinct whole-brain network configurations depending on the stimulation
694 site. Specifically, networks following TMS over EVA exhibited higher small-worldness—a
695 topological property characterized by strong local clustering and short path lengths—
696 compared to those following TMS over MT. This network architecture is thought to
697 support efficient parallel information processing by maximizing information transfer at
698 minimal wiring cost (Achard & Bullmore, 2007). The clustered, locally efficient
699 organization of the $TMS_{(EVA)}$ network may promote functional resilience and flexible
700 redistribution of activity. This could help explain the relative preservation of behavioral

701 performance during late TMS onset, suggesting that the network maintains coherence
702 despite transient perturbations (Wu *et al.*, 2020). In contrast, the more dispersed
703 $TMS_{(MT)}$ network configuration likely reflects broader propagation of task-specific
704 interference across higher-order visual regions, potentially leading to a less efficient,
705 more vulnerable network state. Congruently, the variable that best accounted for the
706 TMS-induced performance impairments following $TMS_{(MT)}$ was the clustering coefficient.
707 This measure reflects the tendency of nodes within a network to form tightly
708 interconnected clusters. High clustering values indicate a well-organized, locally efficient
709 network structure, whereas lower values reflect a more random or fragmented
710 configuration, consistent with patterns observed in our ICA analyses. Our findings
711 showed that participants who exhibited greater performance declines had lower
712 clustering coefficients, suggesting that a more dispersed network organization is
713 detrimental to motion direction discrimination. It would be valuable in future work to
714 investigate whether these network disruptions extend to other visual subfunctions—or
715 even domain-general cognitive functions—in order to determine the broader functional
716 impact of focal perturbations on brain-wide network dynamics.

717 This result fits with our initial hypothesis which was that EVA, given its role as an
718 early-stage integrative cortical area, would maintain more stable synaptic and network
719 dynamics in response to TMS, resulting in greater resistance to externally induced
720 disruptions in both perceptual performance and functional connectivity compared to
721 MT. It is in line with a modelling study, showing that brain hubs, where activity is
722 integrated and further distributed (like EVA in our case) operate in a slower regime and
723 appear to be functionally less affected by focal perturbations (Gollo *et al.*, 2017). In
724 contrast, perturbations of peripheral or more associative areas (e.g., MT), might have
725 greater impact on acute network activity. Lesion studies also provided evidence that
726 damage to the homologue of MT in behaving cats impairs more relearning of motion

727 discrimination and learning transfer than lesions to EVA (Das *et al.*, 2012). To sum up,
728 the network analyses revealed differences between the two disrupted areas, not
729 observable with classical activation analyses. It highlights the relevance of graph-
730 theoretical metrics in capturing functionally meaningful changes in network topology. In
731 particular, the clustering coefficient appears to be a sensitive marker of TMS-induced
732 network reconfiguration and its behavioural consequences.

733

734 **5. Limitations of the current work and open questions:**

735 The aim of this study was to develop a causal connectomic framework for
736 understanding motion direction discrimination by selectively perturbing two key
737 network nodes using TMS. However, it is important to recognize certain methodological
738 limitations inherent to this approach. Unlike brain lesions, TMS-induced perturbations
739 are both temporally transient and spatially focal. More critically, the physiological
740 consequences of a lesion might differ fundamentally from those of TMS. Brain lesions
741 not only disrupt local neuronal activity but also provoke widespread, often nonspecific
742 responses—particularly in the hyperacute phase—such as excitotoxicity, inflammation,
743 and diaschisis (Lai *et al.*, 2014; Farooqui *et al.*, 2022). These processes can profoundly
744 alter interregional communication through mechanisms unrelated to normal synaptic
745 signaling.

746 In contrast, the type of TMS used in this study induces neuronal firing and inter-
747 areal communication, though likely mediated by different—and possibly more
748 superficial or excitatory—neuronal populations than those affected by a brain lesion.
749 This distinction is essential when interpreting the resulting BOLD signal changes. While
750 increases in BOLD activity are often taken to reflect compensatory engagement, they
751 could alternatively indicate maladaptive or inefficient network recruitment. Future work

752 using population tuning models or decoding approaches could help clarify the functional
753 relevance of these activations and determine whether they truly reflect adaptive
754 reorganization or instead a signature of disrupted processing.

755 Another intriguing aspect concerns the resting-state TMS-fMRI data (presented
756 in the supplementary results). These results helped confirm the spatial specificity of the
757 TMS effects, validating that stimulation targeted the intended network nodes even at
758 rest. However, we observed that the direction of BOLD signal changes at rest contrasted
759 with those seen during task performance. This apparent discrepancy has been reported
760 in prior studies and may reflect state-dependent effects of TMS—that is, the neural
761 response to TMS can differ markedly depending on whether the brain is at rest or
762 engaged in a task. Another contributing factor could be the experimental design itself:
763 we employed a block design during the resting-state acquisition and an event-related
764 design during the task-based sessions. These methodological differences could influence
765 the temporal integration of BOLD responses and the observed directionality of signal
766 change (Chee *et al.*, 2003; Tie *et al.*, 2009). Together, these findings underscore the
767 complexity of interpreting TMS-induced effects in fMRI data and highlight the need to
768 consider both brain state and experimental context when drawing causal inferences.

769

770 **6. Conclusion**

771 Despite growing interest and significant advances in computational modelling,
772 the causal mechanisms underlying neural network dynamics following a lesion remain
773 incompletely understood. In this study, we employed concurrent TMS-fMRI to probe the
774 neural mechanisms supporting functional reorganization across whole-brain networks,
775 using a targeted perturbation approach.

Our findings offer neuroimaging evidence for the context-dependent nature of TMS effects, suggesting that such perturbations may preferentially engage specific neuronal populations depending on task demands. Moreover, we show that inducing focal, virtual lesions at different levels of the visual hierarchy leads to distinct patterns of dysregulation across visual networks.

Complementing classical lesion studies (Das *et al.*, 2012), our results highlight the utility of TMS-fMRI coupling as a powerful tool for investigating 'causal disconnectomics'—the causal relationships between localized disruptions and large-scale neural and behavioural consequences (Egger *et al.*, 2021). This approach holds promise for precisely mapping how local perturbations propagate through brain networks, especially when assessed during active cognitive processing. Ultimately, such techniques may advance our understanding of brain resilience, compensation, and vulnerability in the face of focal damage.

Acknowledgements:

We thank Holly Bridge for her insightful comments on the manuscript. We would like to thank the MRI and neuromodulation facilities of the Human Neuroscience Platform of the Fondation Campus Biotech Geneva, for technical advice. This study was supported by the Bertarelli Foundation (Catalyst BC77O7 to FCH & ER), by the Swiss National Science Foundation (PRIMA PR00P3_179867 to ER), and by the Defitech Foundation (to FCH).

Conflict of interest statement: The authors declare no financial or non-financial competing interests.

References

Abed Rabbo F, Koch G, Lefèvre C & Seizeur R (2015). Direct geniculo-extrastriate pathways: a review of the literature. *Surg Radiol Anat SRA* **37,** 891–899.

Achard S & Bullmore E (2007). Efficiency and cost of economical brain functional networks. *PLoS Comput Biol* **3,** e17.

Ajina S, Pestilli F, Rokem A, Kennard C & Bridge H (2015). Human blindsight is mediated by an intact geniculo-extrastriate pathway. *eLife* **4,** e08935.

d'Alfonso AA, van Honk J, Schutter DJ, Caffé AR, Postma A & de Haan EH (2002). Spatial and temporal characteristics of visual motion perception involving V5 visual cortex. *Neurol Res* **24,** 266–270.

Andersson JLR, Hutton C, Ashburner J, Turner R & Friston K (2001). Modeling Geometric Deformations in EPI Time Series. *NeuroImage* **13,** 903–919.

Ashburner J & Friston KJ (2005). Unified segmentation. *NeuroImage* **26,** 839–851.

Bancroft TD, Hogeveen J, Hockley WE & Servos P (2014). TMS-induced neural noise in sensory cortex interferes with short-term memory storage in prefrontal cortex. *Front Comput Neurosci*; DOI: 10.3389/fncom.2014.00023.

Bassett DS & Bullmore ET (2009). Human brain networks in health and disease. *Curr Opin Neurol* **22,** 340–347.

Beckers G & Hömberg V (1992). Cerebral visual motion blindness: transitory akinetopsia induced by transcranial magnetic stimulation of human area V5. *Proc Biol Sci* **249,** 173–178.

Bell AJ & Sejnowski TJ (1995). An information-maximization approach to blind separation and blind deconvolution. *Neural Comput* **7,** 1129–1159.

Bergmann TO, Varatheeswaran R, Hanlon CA, Madsen KH, Thielscher A & Siebner HR (2021). Concurrent TMS-fMRI for causal network perturbation and proof of target engagement. *NeuroImage* **237,** 118093.

Bestmann S. (2008). Mapping Causal Interregional Influences With Concurrent TMS-fMRI - PubMed. *Exp Brain Res*. Available at: https://pubmed.ncbi.nlm.nih.gov/18936922/ [Accessed March 23, 2020].

Beynel L, Appelbaum LG, Luber B, Crowell CA, Hilbig SA, Lim W, Nguyen D, Chrapliwy NA, Davis SW, Cabeza R, Lisanby SH & Deng Z-D (2019). Effects of online repetitive transcranial magnetic stimulation (rTMS) on cognitive processing: A meta-analysis and recommendations for future studies. *Neurosci Biobehav Rev* **107,** 47–58.

Blanco R, Preti MG, Koba C, Ville DVD & Crimi A (2024). Comparing structure–function relationships in brain networks using EEG and fNIRS. *Sci Rep* **14,** 28976.

Born RT & Tootell RBH (1992). Segregation of global and local motion processing in primate middle temporal visual area. *Nature* **357,** 497–499.

Brett M, Anton JL, Valabrgue R & Poline J-B (2002). Region of interest analysis using an SPM toolbox. Presented at the 8th International Conference on Functional Mapping of the Human Brain, June 2-6, 2002, Sendai, Japan. *Neuroimage* **13,** 210–217.

Bridge H, Thomas O, Jbabdi S & Cowey A (2008). Changes in connectivity after visual cortical brain damage underlie altered visual function. *Brain J Neurol* **131,** 1433–1444.

Bullmore E & Sporns O (2012). The economy of brain network organization. *Nat Rev Neurosci* **13,** 336–349.

Calhoun VD, Adali T, Pearlson GD & Pekar JJ (2001). A method for making group inferences from functional MRI data using independent component analysis. *Hum Brain Mapp* **14,** 140–151.

Caparelli EC, Backus W, Telang F, Wang G-J, Maloney T, Goldstein RZ, Anschel D & Henn F (2010). Simultaneous TMS-fMRI of the Visual Cortex Reveals Functional Network, Even in Absence of Phosphene Sensation. *Open Neuroimaging J* **4,** 100–110.

Chee MWL, Venkatraman V, Westphal C & Siong SC (2003). Comparison of block and event-related fMRI designs in evaluating the word-frequency effect. *Hum Brain Mapp* **18,** 186–193.

Chen N, Lu J, Shao H, Weng X & Fang F (2017). Neural mechanisms of motion perceptual learning in noise. *Hum Brain Mapp* **38,** 6029–6042.

Cocchi L, Sale MV, L Gollo L, Bell PT, Nguyen VT, Zalesky A, Breakspear M & Mattingley JB (2016). A hierarchy of timescales explains distinct effects of local inhibition of primary visual cortex and frontal eye fields ed. Culham JC. *eLife* **5,** e15252.

Das A, DeMagistris M & Huxlin KR (2012). Different Properties of Visual Relearning after Damage to Early Versus Higher-Level Visual Cortical Areas. *J Neurosci* **32,** 5414–5425.

Egger P, Evangelista GG, Koch PJ, Park C-H, Levin-Gleba L, Girard G, Beanato E, Lee J, Choirat C, Guggisberg AG, Kim Y-H & Hummel FC (2021). Disconnectomics of the Rich Club Impacts Motor Recovery After Stroke. *Stroke*STROKEAHA120031541.

Farooqui M, Ortega-Gutierrez S, Hernandez K, Torres VO, Dajles A, Zevallos CB, Quispe-Orozco D, Mendez-Ruiz A, Manzel K, Ten Eyck P, Tranel D, Karandikar NJ & Ortega SB (2022). Hyperacute immune responses associate with immediate neuropathology and motor dysfunction in large vessel occlusions. *Ann Clin Transl Neurol* **10,** 276–291.

Fleury L et al. (2022). Toward individualized medicine in stroke-The TiMeS project: Protocol of longitudinal, multi-modal, multi-domain study in stroke. *Front Neurol* **13,** 939640.

Fornito A, Zalesky A & Breakspear M (2015). The connectomics of brain disorders. *Nat Rev Neurosci* **16,** 159–172.

Foss J & Milton J (2000). Multistability in Recurrent Neural Loops Arising From Delay. *J Neurophysiol* **84,** 975–985.

Glick C, Gajawelli N, Sun Y, Badami F, Saggar M & Etkin A (2024). Concurrent single-pulse (sp) TMS/fMRI to reveal the causal connectome in healthy and patient populations. *BioRxiv Prepr Serv Biol*2024.09.25.614833.

Gollo LL, Roberts JA & Cocchi L (2017). Mapping how local perturbations influence systems-level brain dynamics. *NeuroImage* **160,** 97–112.

Grasso PA, Làdavas E, Bertini C, Caltabiano S, Thut G & Morand S (2018). Decoupling of Early V5 Motion Processing from Visual Awareness: A Matter of Velocity as Revealed by Transcranial Magnetic Stimulation. *J Cogn Neurosci* **30,** 1517–1531.

Grossberg S, Mingolla E & Pack C (1999). A neural model of motion processing and visual navigation by cortical area MST. *Cereb Cortex N Y N 1991* **9,** 878–895.

Himberg J, Hyvärinen A & Esposito F (2004). Validating the independent components of neuroimaging time series via clustering and visualization. *NeuroImage* **22,** 1214–1222.

Huang D-W & Yu Z-G (2017). Dynamic-Sensitive centrality of nodes in temporal networks. *Sci Rep* **7,** 41454.

Imani E, Harati A, Pourreza H & Goudarzi MM (2021). Brain-behavior relationships in the perceptual decision-making process through cognitive processing stages. *Neuropsychologia* **155,** 107821.

Jimenez-Marin A, De Bruyn N, Gooijers J, Llera A, Meyer S, Alaerts K, Verheyden G, Swinnen SP & Cortes JM (2022). Multimodal and multidomain lesion network mapping enhances prediction of sensorimotor behavior in stroke patients. *Sci Rep* **12,** 22400.

Joukes J, Hartmann TS & Krekelberg B (2014). Motion detection based on recurrent network dynamics. *Front Syst Neurosci*; DOI: 10.3389/fnsys.2014.00239.

Jung J, Bungert A, Bowtell R & Jackson SR (2020). Modulating Brain Networks With Transcranial Magnetic Stimulation Over the Primary Motor Cortex: A Concurrent TMS/fMRI Study. *Front Hum Neurosci*; DOI: 10.3389/fnhum.2020.00031.

Kennerley SW & Walton ME (2011). Decision Making and Reward in Frontal Cortex. *Behav Neurosci* **125,** 297–317.

Koivisto M, Leino K, Pekkarinen A, Karttunen J, Railo H & Hurme M (2021). Transcranial magnetic stimulation (TMS)-induced Blindsight of Orientation is Degraded Conscious Vision. *Neuroscience*; DOI: 10.1016/j.neuroscience.2021.08.025.

Koivisto M, Mäntylä T & Silvanto J (2010). The role of early visual cortex (V1/V2) in conscious and unconscious visual perception. *NeuroImage* **51,** 828–834.

Kottaram A, Johnston L, Ganella E, Pantelis C, Kotagiri R & Zalesky A (2018). Spatio-temporal dynamics of resting-state brain networks improve single-subject prediction of schizophrenia diagnosis. *Hum Brain Mapp* **39,** 3663–3681.

Lai TW, Zhang S & Wang YT (2014). Excitotoxicity and stroke: Identifying novel targets for neuroprotection. *Prog Neurobiol* **115,** 157–188.

Lamme VA (2001). Blindsight: the role of feedforward and feedback corticocortical connections. *Acta Psychol (Amst)* **107,** 209–228.

Lamme VA & Roelfsema PR (2000). The distinct modes of vision offered by feedforward and recurrent processing. *Trends Neurosci* **23,** 571–579.

Latora V & Marchiori M (2001). Efficient behavior of small-world networks. *Phys Rev Lett* **87,** 198701.

Leitão J, Thielscher A, Tünnerhoff J & Noppeney U (2015). Concurrent TMS-fMRI Reveals Interactions between Dorsal and Ventral Attentional Systems. *J Neurosci* **35,** 11445–11457.

Lim S, Radicchi F, van den Heuvel MP & Sporns O (2019). Discordant attributes of structural and functional brain connectivity in a two-layer multiplex network. *Sci Rep* **9,** 2885.

Lin Z, Nie C, Zhang Y, Chen Y & Yang T (2020). Evidence accumulation for value computation in the prefrontal cortex during decision making. *Proc Natl Acad Sci* **117,** 30728–30737.

Litwińczuk MC, Muhlert N, Cloutman L, Trujillo-Barreto N & Woollams A (2022). Combination of structural and functional connectivity explains unique variation in specific domains of cognitive function. *NeuroImage* **262,** 119531.

Liu LD & Pack CC (2017). The Contribution of Area MT to Visual Motion Perception Depends on Training. *Neuron* **95,** 436-446.e3.

Luo H, Ye X, Cai H-T, Wang M, Wang Y, Liu Q, Xu Y, Mao Z, Cai Y, Hong J, Zhang C, Wei P, Lu Y, Liu Q, Xu J & Yuan T-F (2025). Frequency-specific and state-dependent neural responses to brain stimulation. *Mol Psychiatry* **30,** 2880–2890.

Ma S, Huang T, Qu Y, Chen X, Zhang Y & Zhen Z (2022). An fMRI dataset for whole-body somatotopic mapping in humans. *Sci Data* **9,** 515.

Mineault PJ, Khawaja FA, Butts DA & Pack CC (2012). Hierarchical processing of complex motion along the primate dorsal visual pathway. *Proc Natl Acad Sci* **109,** E972–E980.

Moore T, Rodman HR & Gross CG (2001). Direction of motion discrimination after early lesions of striate cortex (V1) of the macaque monkey. *Proc Natl Acad Sci* **98,** 325–330.

Navarro de Lara LI, Tik M, Woletz M, Frass-Kriegl R, Moser E, Laistler E & Windischberger C (2017). High-sensitivity TMS/fMRI of the Human Motor Cortex Using a Dedicated Multichannel MR Coil. *NeuroImage* **150,** 262–269.

Navarro de Lara LI, Windischberger C, Kuehne A, Woletz M, Sieg J, Bestmann S, Weiskopf N, Strasser B, Moser E & Laistler E (2015). A novel coil array for combined TMS/fMRI experiments at 3 T. *Magn Reson Med* **74,** 1492–1501.

Newsome WT & Paré EB (1988). A selective impairment of motion perception following lesions of the middle temporal visual area (MT). *J Neurosci Off J Soc Neurosci* **8,** 2201–2211.

Offen S, Gardner J, Schluppeck D & Heeger D (2010). Differential roles for frontal eye fields (FEF) and intraparietal sulcus (IPS) in visual working memory and visual attention. *J Vis* **10,** 28.

Ozdemir RA, Tadayon E, Boucher P, Momi D, Karakhanyan KA, Fox MD, Halko MA, Pascual-Leone A, Shafi MM & Santarnecchi E (2020). Individualized perturbation of the human connectome reveals reproducible biomarkers of network dynamics relevant to cognition. *Proc Natl Acad Sci* **117,** 8115–8125.

Papo D, Buldú JM, Boccaletti S & Bullmore ET (2014). Complex network theory and the brain. *Philos Trans R Soc B Biol Sci* **369,** 20130520.

Pascual-Leone A, Bartres-Faz D & Keenan JP (1999). Transcranial magnetic stimulation: studying the brain-behaviour relationship by induction of "virtual lesions." *Philos Trans R Soc Lond B Biol Sci* **354,** 1229–1238.

Perera ND, Wischnewski M, Alekseichuk I, Shirinpour S & Opitz A (2024). State-Dependent Motor Cortex Stimulation Reveals Distinct Mechanisms for Corticospinal Excitability and Cortical Responses. *eNeuro*; DOI: 10.1523/ENEURO.0450-24.2024.

Rafiei F & Rahnev D (2022). TMS Does Not Increase BOLD Activity at the Site of Stimulation: A Review of All Concurrent TMS-fMRI Studies. *eNeuro*; DOI: 10.1523/ENEURO.0163-22.2022.

Ricci R, Salatino A, Li X, Funk A, Logan S, Mu Q, Johnson K, Bohning D & George M (2012). Imaging the neural mechanisms of TMS neglect-like bias in healthy volunteers with the interleaved TMS/fMRI technique: preliminary evidence. *Front Hum Neurosci*; DOI: 10.3389/fnhum.2012.00326.

Romero MC, Davare M, Armendariz M & Janssen P (2019). Neural effects of transcranial magnetic stimulation at the single-cell level. *Nat Commun*; DOI: 10.1038/s41467-019-10638-7.

Rossi S et al. (2021). Safety and recommendations for TMS use in healthy subjects and patient populations, with updates on training, ethical and regulatory issues: Expert Guidelines. *Clin Neurophysiol* **132,** 269–306.

Rubinov M & Sporns O (2010). Complex network measures of brain connectivity: uses and interpretations. *NeuroImage* **52,** 1059–1069.

991 Ruff CC, Blankenburg F, Bjoertomt O, Bestmann S, Freeman E, Haynes J-D, Rees G,
992 Josephs O, Deichmann R & Driver J (2006). Concurrent TMS-fMRI and
993 Psychophysics Reveal Frontal Influences on Human Retinotopic Visual Cortex.
994 *Curr Biol* **16,** 1479–1488.

995 Ruff CC, Blankenburg F, Bjoertomt O, Bestmann S, Weiskopf N & Driver J (2008).
996 Hemispheric Differences in Frontal and Parietal Influences on Human Occipital
997 Cortex: Direct Confirmation with Concurrent TMS–fMRI. *J Cogn Neurosci* **21,**
998 1146–1161.

999 Ruff CC, Driver J & Bestmann S (2009). Combining TMS and fMRI. *Cortex J Devoted Study*
1000 *Nerv Syst Behav* **45,** 1043–1049.

1001 Rust NC, Mante V, Simoncelli EP & Movshon JA (2006). How MT cells analyze the motion
1002 of visual patterns. *Nat Neurosci* **9,** 1421–1431.

1003 Sani I, Stemmann H, Caron B, Bullock D, Stemmler T, Fahle M, Pestilli F & Freiwald WA
1004 (2021). The human endogenous attentional control network includes a ventro-
1005 temporal cortical node. *Nat Commun* **12,** 360.

1006 Schwabe L, Obermayer K, Angelucci A & Bressloff PC (2006). The Role of Feedback in
1007 Shaping the Extra-Classical Receptive Field of Cortical Neurons: A Recurrent
1008 Network Model. *J Neurosci* **26,** 9117–9129.

1009 Shao Z & Burkhalter A (1996). Different Balance of Excitation and Inhibition in Forward
1010 and Feedback Circuits of Rat Visual Cortex. *J Neurosci* **16,** 7353–7365.

1011 Siebner HR et al. (2022). Transcranial magnetic stimulation of the brain: What is
1012 stimulated? – A consensus and critical position paper. *Clin Neurophysiol* **140,**
1013 59–97.

1014 Siegel JS, Ramsey LE, Snyder AZ, Metcalf NV, Chacko RV, Weinberger K, Baldassarre A,
1015 Hacker CD, Shulman GL & Corbetta M (2016). Disruptions of network
1016 connectivity predict impairment in multiple behavioral domains after stroke.
1017 *Proc Natl Acad Sci U S A* **113,** E4367-4376.

1018 Silvanto J & Pascual-Leone A (2008). State-Dependency of Transcranial Magnetic
1019 Stimulation. *Brain Topogr* **21,** 1–10.

1020 Simoncelli EP & Heeger DJ (1998). A model of neuronal responses in visual area MT.
1021 *Vision Res* **38,** 743–761.

1022 Telesford QK, Simpson SL, Burdette JH, Hayasaka S & Laurienti PJ (2011). The Brain as a
1023 Complex System: Using Network Science as a Tool for Understanding the Brain.
1024 *Brain Connect* **1,** 295–308.

1025 Tie Y, Suarez RO, Whalen S, Radmanesh A, Norton IH & Golby AJ (2009). Comparison of
1026 blocked and event-related fMRI designs for pre-surgical language mapping.
1027 *NeuroImage* **47,** T107–T115.

1028 Tu W, Ma Z & Zhang N (2021). Brain network reorganization after targeted attack at a
1029 hub region. *NeuroImage* **237,** 118219.

Tzourio-Mazoyer N, Landeau B, Papathanassiou D, Crivello F, Etard O, Delcroix N, Mazoyer B & Joliot M (2002). Automated anatomical labeling of activations in SPM using a macroscopic anatomical parcellation of the MNI MRI single-subject brain. *NeuroImage* **15,** 273–289.

Vink JJT, Mandija S, Petrov PI, van den Berg CAT, Sommer IEC & Neggers SFW (2018). A novel concurrent TMS-fMRI method to reveal propagation patterns of prefrontal magnetic brain stimulation. *Hum Brain Mapp* **39,** 4580–4592.

Wang J, Wang X, Xia M, Liao X, Evans A & He Y (2015). Corrigendum: GRETNA: a graph theoretical network analysis toolbox for imaging connectomics. *Front Hum Neurosci*. Available at: https://www.frontiersin.org/articles/10.3389/fnhum.2015.00458 [Accessed July 23, 2022].

Wongtrakun J, Zhou S-H, O'Connell RG, Chong TT-J, Bellgrove MA & Coxon JP (2025). The role of human intraparietal sulcus in evidence accumulation revealed by EEG and model-informed fMRI. 2025.02.05.636628. Available at: https://www.biorxiv.org/content/10.1101/2025.02.05.636628v2 [Accessed June 13, 2025].

Wu YK, Hengen KB, Turrigiano GG & Gjorgjieva J (2020). Homeostatic mechanisms regulate distinct aspects of cortical circuit dynamics. *Proc Natl Acad Sci* **117,** 24514–24525.

Zhang Z, Yin C & Yang T (2022). Evidence accumulation occurs locally in the parietal cortex. *Nat Commun* **13,** 4426.

Zhao X, Tian L, Yan J, Yue W, Yan H & Zhang D (2017). Abnormal Rich-Club Organization Associated with Compromised Cognitive Function in Patients with Schizophrenia and Their Unaffected Parents. *Neurosci Bull* **33,** 445–454.

1058